processes

MDPI

Article

Efficiency of Electrochemical Methods of Purification and Control over the Oxide Concentration in Halide Melts: $PbCl_2$

Andrey Nikolaev, Albert Mullabaev, Andrey Suzdaltsev * and Yuriy P. Zaikov

Scientific-Research Department of Electrolysis, Institute of High Temperature Electrochemistry UB RAS, Akademicheskaya St. 20, 620066 Yekaterinburg, Russia
* Correspondence: suzdaltsev_av@ihte.uran.ru

Abstract: The purification of molten salts from admixtures as well as the effective control of admixture concentration has attracted researchers' interests. In the present paper, the possibility of the electrochemical purification of $PbCl_2$ from PbO and the effective control over the oxide ions concentration in molten $PbCl_2$ is studied at the temperature of 520 °C. The $PbCl_2$ melt with the initial addition of 0.5 wt% of PbO was used as a molten salt sample. The method of potentiostatic electrolysis was used to remove the oxide additions from the melt; the linear and square-wave voltammetry dependencies were recorded, and the melt samples were taken for analysis. Based both on the results of the electrochemical measurements and the analysis of oxygen concentration in the electrolyte, we built linear empirical dependencies of the anode peak current of the oxidation of oxygen-containing electroactive anions on the PbO concentration in the studied melt. We demonstrated that the obtained dependencies may be used for direct electrochemical nondestructive in-situ control over the concentration of PbO dissolved in the $PbCl_2$ melt containing up to 0.5 wt% of PbO. The deep electrochemical purification of the chloride $PbCl_2$ melt from molten oxide (up to 0.044 wt% PbO or to 0.007 wt% of oxygen) was achieved by the potentiostatic electrolysis.

Keywords: halide melt; salts purity; $PbCl_2$-PbO; electrochemical purification; electrochemical analysis; oxide concentration; voltammetry

Citation: Nikolaev, A.; Mullabaev, A.; Suzdaltsev, A.; Zaikov, Y.P. Efficiency of Electrochemical Methods of Purification and Control over the Oxide Concentration in Halide Melts: $PbCl_2$. *Processes* **2023**, *11*, 636. https://doi.org/10.3390/pr11020636

Academic Editor: Ioannis Spanopoulos

Received: 25 January 2023
Revised: 14 February 2023
Accepted: 18 February 2023
Published: 19 February 2023

1. Introduction

Molten salts have been widely used for production of metals, alloys, and functional materials for more than two hundred years [1–3]. Moreover, recently, molten salts have been actively studied for application in nuclear (molten salt reactors) and non-nuclear (thermal solar cells) low-power reactors [4–7]. The composition and purity of molten salts have always been under tight inspection, especially if they were intended for the production of nuclear reactor materials (liquid metal and liquid salt coolants: Pb, Na, LiF–BeF_2, LiF–NaF–KF, etc. [8,9]) or for spent nuclear fuel reprocessing (LiCl, LiCl–KCl, etc.) within the frame of the closed nuclear fuel cycle [10–15]. Any excess of admixtures in molten salts used for the above processes may result in [16–20]:

- Escalation of nuclear waste and additional complex processing procedures;
- Changes in the process parameters and possible disruption of the process control;
- Increased corrosion of the reactor materials and decrease in the reactor operation life;
- Contamination of the target products and decline in the process efficiency.

These factors are especially vital in the industrial implementation of the developed technologies.

The purification of molten salts from admixtures, as well as the effective control over the admixture's concentrations, are of interest from different points of view.

The purification of the molten salts can be achieved by a number of methods, including vacuum drying [21], chlorination [18,22], electrolysis [23,24], zone recrystallization [25,26], etc. However, both after the preparation of the media and during operations using real objects, constant monitoring of the admixture's concentration is required. Even a negligible change

in the molten salt's composition can cause changes in their physical-chemical properties and in those of the target products [27–30].

Inductively coupled plasma–mass spectrometry (ICP-MS) and inductively coupled plasma–optical emission spectrometry (ICP-OES) are the most accurate and precise methods for determining minor element concentrations [31–34]. The advantages of these methods are wide recognition, high accuracy and sensitivity (up to the nanomolar level), simultaneous determination of the content of several elements (including isotopes (ICP MS)), long linear calibration range, etc. However, since these methods use aqueous solutions of the samples, they cannot be used to determine the content of moisture and a number of oxides (in particular, Li_2O in LiCl, PbO in $PbCl_2$, etc.). Moreover, the equipment used for analysis is expensive and requires increased cleanliness of the process media (which is often impossible during the industrial operation). Such methods also require additional time to prepare the sample and to perform other operations. Therefore, these methods of analysis are not suitable for the real-time analysis of the samples.

For oxides with strongly acidic or basic properties, chemical titration methods and pH measurements can be used [35], but they are also time-consuming and not suitable for oxides that are not strongly acidic or basic (e.g., PbO).

Electrochemical methods are promising both for removing and controlling the content of admixtures in molten salts. The disadvantages of such methods are a relatively lower sensitivity (in comparison with ICP methods) and the complexity of results interpretation in systems containing several different admixtures.

On the other hand, the advantages of the electrochemical methods for the substances analysis include:

- Portable equipment;
- Relatively cheap consumable electrode materials;
- Possibility of direct measurement both in laboratory and industrial reactors;
- Rapid in-situ multiple analysis;
- Theoretical background of the methods;
- The electrochemical sensor placed directly in the reactor allows for eliminating its depressurization during the analysis.

For example, at present, electrochemical sensors for determining the content of elements in background electrolytes in the range of up to 10 wt% [36–47] are widely studied, while the data on the determination of low oxygen concentrations (hundreds of ppm) are limited [46–48]. Basically, these methods were mainly used to determine the concentration of oxide ions in the fluoride melts intended for electrolytic aluminium production (NaF–AlF_3–Al_2O_3, KF–AlF_3–Al_2O_3) or coolants in molten salt reactors (LiF–BeF_2, LiF–NaF–KF). Far less attention has been devoted to the determination of admixtures in chloride melts.

In the present work, the possibility of deep electrochemical purification of a halide melt ($PbCl_2$) and the sensitivity of electrochemical control over the oxide content in it are studied. The electrochemical method was chosen because it seems to be the only method of the in-situ control of the molten salt composition at the moment. The $PbCl_2$ melt was chosen for testing and determining the accuracy of the technique due to the fact that there are comprehensive data on its physicochemical properties, as well as on the mechanisms of the electrode processes within it [49–53]. Moreover, to date, $PbCl_2$ has been considered as one of the most promising chlorinating agents in pyrochemical stages of spent nuclear fuel processing [9,54–57].

2. Materials and Methods

Process flow. To achieve the goals of the work, the experiment was carried out according to the following scheme. PbO (0.5 wt%) was added to a $PbCl_2$ melt preliminarily purified from oxide admixtures, and the increasing concentration of dissolved electroactive oxygen ions in the melt was controlled by the electrochemical measurements. The dissolution of the PbO sample in the melt was determined according to the stabilization of the current on the recorded voltammograms. After that, the obtained $PbCl_2$–PbO melt was gradually

purified from oxygen ions using potentiostatic electrolysis. The electrolysis was periodically interrupted to perform electrochemical measurements in the melt. At the moment of the current interruption, the samples of the melt were taken for an analysis of the oxygen content by independent methods. The duration of electrolysis was estimated according to the Faraday law, taking into account the 100% anode current efficiency. At the end of the experiment, the results of electrochemical measurements and the results of the independent analysis of the oxide content of the melt were compared.

Melt preparation. The melt was prepared using commercial $PbCl_2$ (>99.8 wt%, JSC Vekton, Russia), which was not preliminarily subjected to any additional purification. Commercial PbO oxide (>99.8 wt%, JSC Vekton, Saint Petersburg, Russia) in the amount of 0.5 wt% was added to molten $PbCl_2$ during measurements.

Experimental setup. The measurements were carried out in a quartz retort with a purified argon atmosphere (see Figure 1). The retort was tightly closed with a fluoroplastic (PTFE) lid, with fittings for electrodes, thermocouples, and gas filling/removal system. The retort was connected to a vacuum pump and to a system of gas supply and purification. A glass-like carbon crucible with a $PbCl_2$ initial salt was placed on the bottom of the retort. The retort was located in a resistance furnace with SiC heaters, vacuumed for 4 h, and heated to the operating temperature under the argon flow. The quality of the salt preparation and the atmosphere in the quartz retort were monitored by the ionization of a thermal vacuum meter and gas sensors (Meradat, Perm, Russia). The temperature of the melt was set, measured, and maintained within ±1 °C by means of a Pt–Pt(10 wt%Rh) thermocouple and a thermocouple module USB-TC01 (National Instruments, Austin, TX, USA). All measurements were performed at the temperature of 520 °C, as the salt melting point was 501 °C [50,51]).

Figure 1. Photograph of the experimental cell.

During the experiment the melt was sampled through an argon outlet by means of quartz tubes, in order to analyze the oxygen content in the melt. After sampling, the tubes were plugged with stoppers made of vacuum rubber and stored in an argon glove box.

Electrochemical measurements. Cyclic voltammetry (CV) and square-wave voltammetry (SWV) procedures using a PGSTAT AutoLab 320N and the NOVA 1.12 software (The MetrOhm, Schiedam, The Netherlands) were applied as electrochemical methods of analysis. These methods imply the polarization of the working electrode and recording the voltammetry dependence, where the value of the current density peak of the studied process is determined by the concentration of the electroactive oxide anions in the melt. The main difference in these methods is that during CV measurements, the working electrode is polarized linearly, whereas during the SWV ones, the electrode potential shifts under the pulsed regime [41,58]. An immersed cylindrical rod made of glass-like carbon (SU-2000, surface 0.9 cm^2, screened with boron nitride) was used as the working electrode (WE); a

rod made of spectrally pure graphite served as the counter electrode (CE); and lead at the bottom of the glass-like carbon crucible served as the reference electrode (RE).

Analysis of oxide concentration in the melt. Along with the electrochemical measurements, the content of dissolved oxide in the melt was determined by independent methods. We have previously mentioned that neither spectral (ICP-OES, ICP-MS) methods nor chemical titration may be used to analyze the concentration of PbO in $PbCl_2$. That is why the methods of carbothermal analysis and nuclear microanalysis were chosen. We have successfully used them before [37,59]. The carbothermal analysis (O analysis) implies the carbothermal reduction of oxide from the $PbCl_2$–PbO samples up to metallic lead, and the determination of the amount of evolved CO during the process. The parameters of the carbothermal reduction were calibrated during the preliminary analysis, with the reference $PbCl_2$–PbO samples containing a known amount of PbO. An OH 836 analyzer (LECO Corp., St. Joseph, MI, USA) was used.

The nuclear microanalysis (NMA) includes the registration of the amount of nuclear reactions between the elementary particles (*d*,*p*0) and the studied $PbCl_2$–PbO samples. We used a 2 MV van de Graaf generator (Institute of Metal Physics UB RAS, Russia) with an accuracy of 2 rel% [60,61].

3. Results

Electrochemical analysis.

Figures 2 and 3 illustrate the current-voltage dependences obtained by cyclic voltammetry and square-wave voltammetry on a glass-like carbon WE in the initial $PbCl_2$ melt at the temperature of 520 °C. Due to the fact that the initial salts nearly always contain oxide admixtures, the oxidation of oxygen-containing anions is observed on the CV dependences at potentials more positive than 0.6 V, relative to the potentials of the lead RE. In this case, two peaks (waves)—$\mathbf{O_I}$ and $\mathbf{O_{II}}$—are formed, which can be associated with a stepwise electrochemical oxidation of oxygen-containing anions via reactions [62,63]:

$$\mathbf{O_I}: O^{2-} + xC = C_xO_{(ads)} + 2e^- \quad (1)$$

$$\mathbf{O_{II}}: O^{2-} + C_xO_{(ads)} = CO_{2(gas)} + 2e^- \quad (2)$$

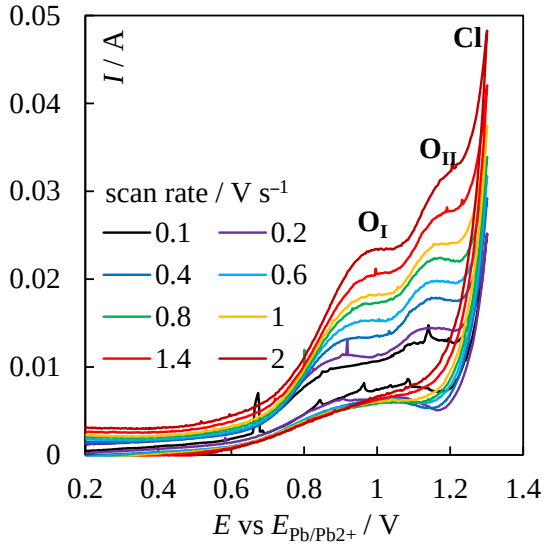

Figure 2. CVs in the initial $PbCl_2$ melt without the external addition of PbO at a potential sweep rate from 0.1 to 2 V s^{-1} and a temperature of 520 °C.

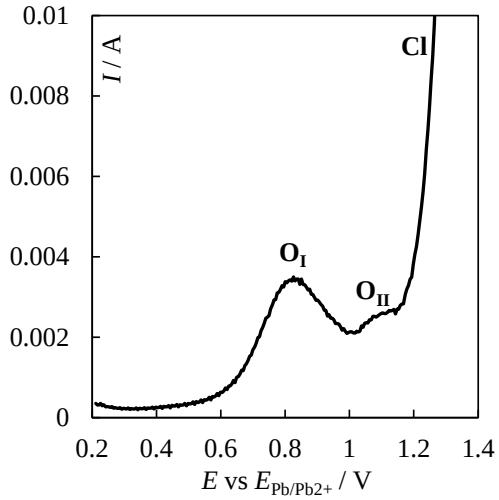

Figure 3. SWV in the initial $PbCl_2$ melt without the external addition of PbO at a potential reverse frequency of 25 Hz, potential sweep rate of 0.1 V s^{-1} and a temperature of 520 °C.

The summarized reaction during electrolysis has the following form:

$$PbO + 0.5C = Pb + CO_{2(gas)} \quad (3)$$

The voltage of the decomposition for this reaction at the temperature of 520 °C is about 0.6 V [64].

At potentials more positive than 1.20 V, a sharp increase in the anode current is observed (wave **Cl**), which is associated with the oxidation of chlorine anions:

$$\mathbf{Cl}\text{: } 2Cl^- = Cl_{2(gas)} + 2e^- \quad (4)$$

This is close to the calculated value of the lead chloride decomposition voltage at the research temperature, which is 1.26 V [64]. In this case reaction, (3) continues if the corresponding oxygen-containing electroactive ions are present in the near anode layer. However, the summarized $PbCl_2$ decomposition reaction prevails [62–64]:

$$PbCl_2 = Pb + Cl_{2(gas)} \quad (5)$$

Similar patterns of the studied process on the glass-like carbon WE may be observed in the analysis of the SWV dependence obtained by the method of square-wave voltammetry (Figure 3). In this case, more distinct peaks of the oxidation of oxygen-containing anions are formed on SWV as opposed to CV.

The dependences presented in Figures 2 and 3 verify that the proposed electrochemical method of analysis can be used to determine oxygen-containing anions in the melt. To analyze the effect of the concentration of dissolved oxygen-containing anions in the melt on their oxidation currents, CV and SWV were obtained in the $PbCl_2$ melt containing 0.5 wt% of PbO. For measurements, a potential sweep rate of 0.1 V s^{-1} (25 Hz with a reverse amplitude of 20 mV in a case of SWV) was chosen.

To choose the parameters of the following measurements and to determine the nature of the limiting stage of the studied electrochemical process, the voltammetry dependences were recorded at different potential sweep rates (Figure 2). It is seen that the potentials of O_I and O_{II} remain almost unchanged, and the current peaks grow as the potential sweep rate increases. This elucidates that processes (1) and (2) are reversible, and the diffusion of the oxygen-containing ions from the melt volume to the WE surface is the limiting factor. In this case, the value of the current peak in a certain interval will be linearly dependent on the PbO concentration in the melt [37,40]. Figure 2 illustrates that any potential sweep rates may be used for the further electrochemical measurements.

At the end of the electrochemical measurements, the initial melt was sampled and PbO amounting to 0.5 wt.% was loaded into the melt. After complete oxide dissolution, the measurements were repeated. In addition, the completeness of the PbO dissolution was verified by the absence of the current peak growth on the recorded voltammetry dependences.

The results are illustrated in Figures 4 and 5. The obtained CV and SWV dependencies demonstrate that the oxidation currents of oxygen-containing anions, when 0.5 wt% of PbO was added to the melt, increased from 0.013 to 0.082 and from 0.003 to 0.014 A, respectively, under otherwise equal conditions. Therefore, the chosen method makes it possible to estimate the content of dissolved oxygen-containing anions in the melt not only qualitatively, but also quantitatively.

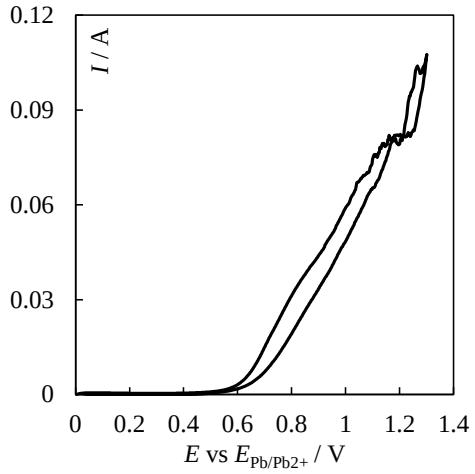

Figure 4. CV in the $PbCl_2$ melt containing 0.5 wt% of PbO at a potential sweep rate of 0.1 V s^{-1} and a temperature of 520 °C.

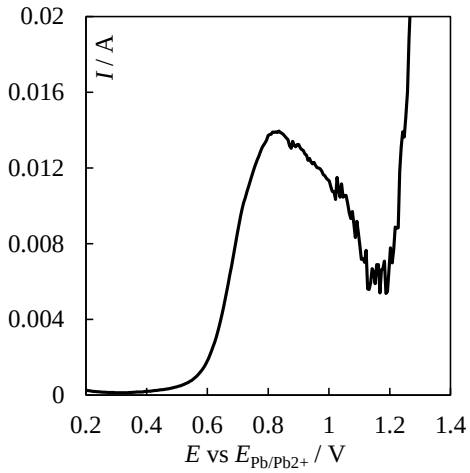

Figure 5. SWV in the $PbCl_2$ melt containing 0.5 wt% of PbO at a potential reverse frequency of 25 Hz, amplitude of 20 mV, potential sweep rate of 0.1 V s^{-1} and a temperature of 520 °C.

For this purpose, by analogy with works [36–41], an empirical dependence of the oxidation peak current of oxygen-containing anions on their concentration in the melt, determined by an independent method of analysis, may be obtained. In this work, such dependence is plotted for the PbO concentrations in $PbCl_2$ up to 0.5 wt% (see below), since the sensitivity of the selected electrochemical method for determining oxygen is considered in the article.

Electrochemical purification of the $PbCl_2$ melt. The purification of the $PbCl_2$–PbO melt from oxygen (oxygen-containing anions) was carried out by the potentiostatic electrolysis of the melt at a potential of 1.0 V. The electrolysis was periodically interrupted to record

current-voltage dependences and to sample the melt for oxide content analysis. This was done in order to build an empirical dependence of the anode O^{2-} oxidation peak current on the PbO content in the melt.

Figure 6 presents the change in the electrolysis current over time and the amount of electricity passed, and Table 1 shows the content of oxygen and PbO in the melt samples during the electrolysis. During electrolysis at the selected anode potential, the current decreased from 0.440 to a constant value of about 0.016–0.018 A. The PbO content in the melt was 0.058 wt%. The absence of a further decrease in current may be explained by:

- Dissolution of oxygen formed at the anode in the melt;
- Oxidation of oxygen-containing anions with relatively strong bonds [65] only at potentials more positive than 1.0 V;
- Side reduction of oxygen dissolved in the melt at the cathode.

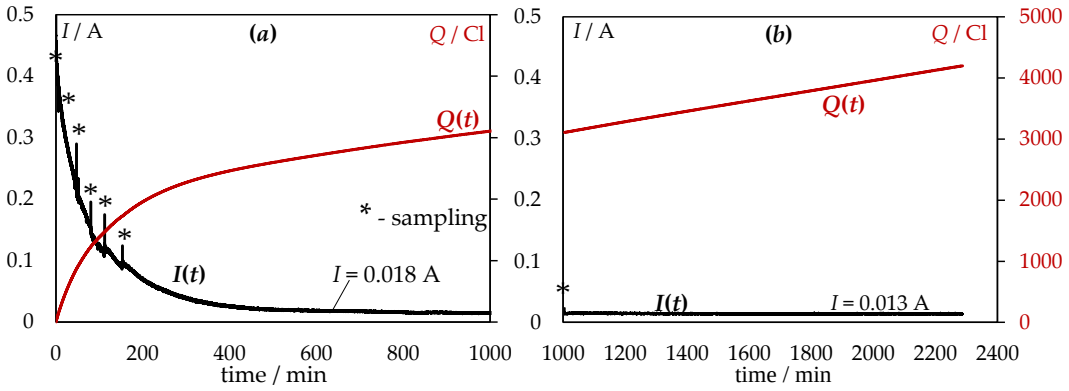

Figure 6. Change in current and amount of electricity passed during the electrolysis of the $PbCl_2$ melt containing 0.5 wt% of PbO at cathode potentials of 1.0 (**a**) and 1.2 (**b**) V.

Table 1. Results of oxygen analysis in the $PbCl_2$-PbO melt.

№	Set Amount of PbO, wt% (Expected)	Electrochemical Analysis		Concentration of PbO, wt%, according to the Analytical Data		Concentration of O, wt%
		* I_p/mA	** δI_p/mA	O Analysis	NMA	O Analysis
-	0 ($PbCl_2$ salt)	-	-	0.067 ± 0.012	-	0.011 ± 0.001
-	0 ($PbCl_2$ melted in air)	-	-	0.096 ± 0.011	-	0.015 ± 0.001
1	0 ($PbCl_2$ melted in Ar)	13.1 ± 0.4	3.3 ± 0.2	0.076 ± 0.014	0.14 ± 0.02	0.012 ± 0.002
2	0.5	81.4 ± 0.4	13.9 ± 0.1	0.349 ± 0.022	0.18 ± 0.03	0.056 ± 0.003
3	0.25	40.0 ± 0.5	10.7 ± 0.1	0.225 ± 0.019	0.11 ± 0.02	0.036 ± 0.003
4	0.14	31.7 ± 0.3	9.0 ± 0.1	0.191 ± 0.014	0.10 ± 0.02	0.030 ± 0.002
5	0.08	25.6 ± 0.4	7.5 ± 0.2	0.138 ± 0.015	0.11 ± 0.01	0.022 ± 0.002
6	0.001	21.4 ± 0.2	5.7 ± 0.1	0.087 ± 0.013	0.08 ± 0.01	0.014 ± 0.002
7	0	11.2 ± 0.2	2.2 ± 0.1	0.058 ± 0.012	0.07 ± 0.02	0.009 ± 0.001
8	0	5.8 ± 0.3	1.8 ± 0.1	0.044 ± 0.012	0.06 ± 0.02	0.007 ± 0.001

* from CVs, obtained at a potential scan rate of 0.1 V s^{-1}; ** from SWVs, obtained at a potential reverse frequency of 25 Hz (scan rate of 0.125 V s^{-1}).

In this regard, the electrolysis was continued at an electrode potential of 1.2 V (close to the potential of chlorine discharge). As a result, the residual oxidation current of oxygen-containing anions was 0.013 A; in addition, according to the carbothermal analysis, about 0.044 wt% of PbO remained in the melt. A total of 4200 C of electricity was passed.

Figures 7 and 8 present the current-voltage dependences recorded during the electrolysis of the $PbCl_2$–PbO melt. There are clear peaks, which show that magnitude decreases

during the electrolysis as a result of a decrease in the PbO content in the melt. Consequently, the recorded peak values of the anode current up to the potential of the oxidation of chlorine ions are explained by the diffusion difficulties in the delivery of electroactive oxygen-containing anions to the anode. In this case, certain current peaks can be described by a linear PbO concentration dependence, crossing the origin, as seen in Figure 9.

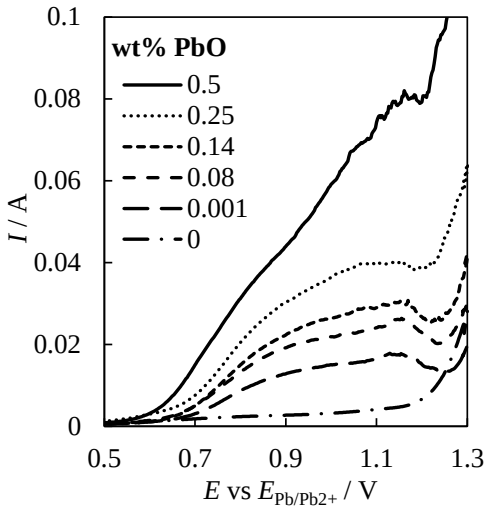

Figure 7. CVs in the $PbCl_2$ melt with a different expected PbO content at a potential sweep rate of 0.1 V s^{-1} and a temperature of 520 °C.

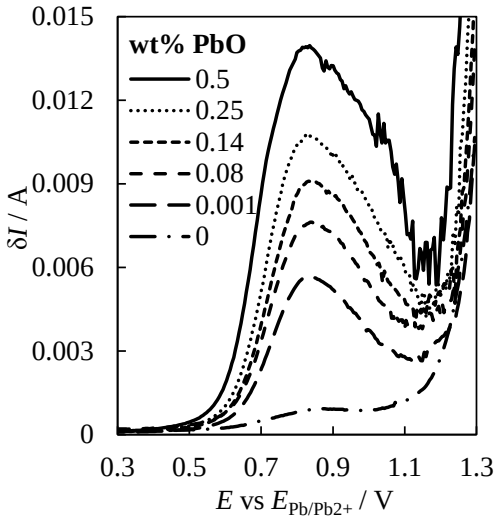

Figure 8. SWVs in the $PbCl_2$ melt with a different expected PbO content at a potential sweep rate of 0.1 V s^{-1} and a temperature of 520 °C.

To build the empirical dependences of the peak values of the oxidation current of oxygen-containing anions on the glass-like carbon WE on the content of dissolved PbO in the $PbCl_2$ melt, we used carbothermal analysis (O analysis) and nuclear microanalysis (NMA). The obtained results, as well as the data on the electrochemical analysis, are summarized in Table 1. The empirical dependences in Figure 9 were built while taking into account the data from the carbothermal analysis.

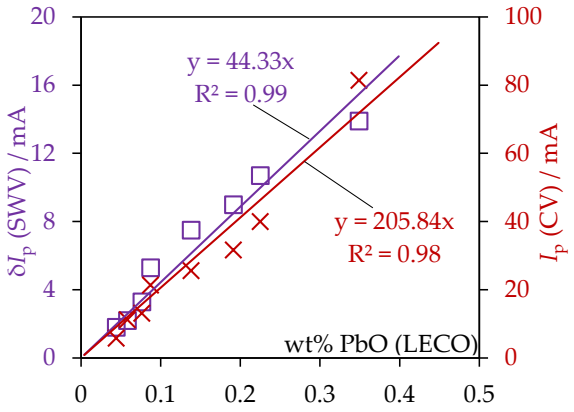

Figure 9. Dependences of the peak values of the anode current of the current-voltage dependences on the PbO concentration in the $PbCl_2$–PbO melt.

It should be noted that when determining the concentration of dissolved oxide in halide melts, the results of carbothermal analysis and nuclear microanalysis can be overestimated, because undissolved oxide (carbothermal analysis) [37] and the presence of light elements in the samples (nuclear microanalysis) are considered [60].

Figures 7–9 elucidate the fact that, in contrast to CVs, SWVs have clear peaks in the oxidation of oxygen-containing anions, even when there is a decrease in the PbO content in the melt below 0.044 wt% (or 0.007 wt% in terms of oxygen). This indicates the high sensitivity of the SWV method in determining the content of dissolved oxide in the melt.

To analyze the sensitivity of the methods used with respect to the dissolved oxide in the melt, the measurements were carried out at a PbO concentration of 0.058 wt% in the melt by varying the rate of the anodic polarization of the working electrode. Figures 10 and 11 show a series of current-voltage dependences obtained at different sweep rates (CVs) or potential reverse frequencies (SWVs). It can be seen that an increase in the rate of anode polarization leads to an increase in anode currents, while determining the peak value of the anode current becomes difficult (especially from the CVs). Therefore, to analyze the content of dissolved oxide in the melts by means of cyclic voltammetry, the measurements must be carried out at the potential sweep rates of 0.1 V s^{-1} and lower. On the other hand, the SWV method is more sensitive to the oxide content in the melt in a wider range of polarization rates (potential reverse frequencies).

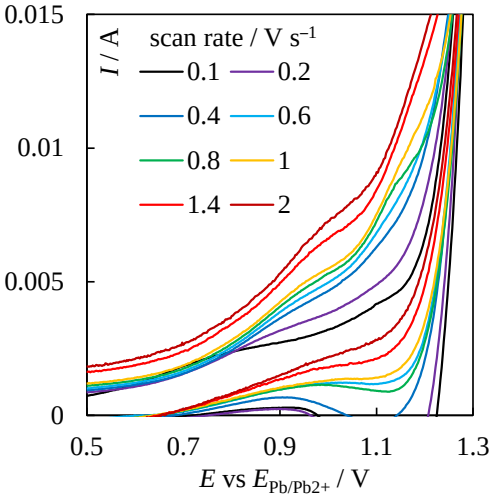

Figure 10. CVs in the $PbCl_2$–0.044 wt% PbO melt at a potential sweep rate from 0.1 to 2 V s^{-1} and a temperature of 520 °C.

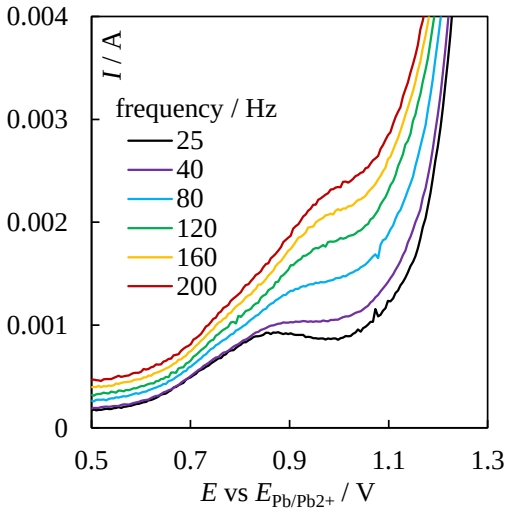

Figure 11. SWV in the $PbCl_2$–0.044 wt% PbO melt at a potential reverse frequency ranging from 25 to 200 Hz, amplitude 20 mV, and a temperature of 520 °C.

The presented results indicate the fundamental possibility of using electrochemical methods for the purification and analysis of the dissolved PbO content in the $PbCl_2$ melt. Similar regularities could be observed in other halide melts, while the electrode materials for measurements should be selected while taking into account the characteristics of a particular melt.

Further work will be devoted to the practical application of the obtained results and to the development of a technique for the detailed analysis and control of oxide concentration in other halide melts.

4. Conclusions

The possibility of purifying and controlling the content of dissolved oxide in molten lead chloride containing PbO (0.5 wt%) was experimentally studied using electrochemical methods of analysis. For this purpose, current-voltage dependences characterizing the peak currents of the anode oxidation of oxygen-containing electroactive anions in the $PbCl_2$ melt, with different contents of dissolved PbO, were obtained by cyclic voltammetry and square-wave voltammetry on a glass-like carbon electrode. In parallel, the independent methods of carbothermal reduction and nuclear microanalysis were used to determine the actual content of dissolved oxide in the melt under study. On the basis of the acquired data, we obtained the linear empirical dependences of the peak values of the oxygen-containing anion oxidation current on glass-like carbon electrodes, depending on the known content of PbO in the $PbCl_2$ melt. The obtained dependences can be used for the direct electrochemical nondestructive in-situ control of the dissolved oxide content in the $PbCl_2$ melt with a PbO content of up to 0.5 wt% and higher.

It is verified that the deep electrochemical purification of the chloride $PbCl_2$ melt from dissolved oxide PbO (up to 0.044 wt% PbO or 0.007 wt% oxygen) can be achieved by potentiostatic electrolysis.

The obtained results may be used to control the PbO concentration in $PbCl_2$ melts, as well as to purify and control other halide melts.

Author Contributions: Conceptualization, A.S. and Y.P.Z.; methodology, A.N. and A.M.; software, A.M.; validation, A.M. and A.N.; formal analysis, A.N.; investigation, A.N. and A.M.; resources, Y.P.Z.; data curation, A.S.; writing—original draft preparation, A.S.; writing—review and editing, A.S. and A.M.; visualization, A.S.; supervision, A.S.; project administration, Y.P.Z.; funding acquisition, Y.P.Z. All authors have read and agreed to the published version of the manuscript.

Funding: This research received no external funding.

Data Availability Statement: The data presented in this study are available on request from the corresponding author.

Acknowledgments: We are grateful to our dear colleagues Vladimir Vykhodets and Tatyana Kurennykh (Institute of Metal Physics UB RAS) for nuclear microanalysis of the samples, as well as to Olga Pavlenko (Institute of High Temperature Electrochemistry UB RAS) for carbothermal analysis of the samples.

Conflicts of Interest: The authors declare no conflict of interest.

References

1. Zaikov, Y.; Batukhtin, V.; Shurov, N.; Suzdaltsev, A. High-Temperature Electrochemistry of Calcium. *Electrochem. Mat. Techn.* **2022**, *1*, 20221007. [CrossRef]
2. Stulov, Y.; Dolmatov, V.; Dubrovskiy, A.; Kuznetsov, S. Electrochemical Synthesis of Functional Coatings and Nanomaterials in Molten Salts and Their Application. *Coatings* **2023**, *13*, 352. [CrossRef]
3. Kushkhov, K.; Kardanova, R.; Kholkina, A. Peculiarities of Holmium and Iron Triad Ions Co-Reduction: Formation of Ho_xNi_y (Ho_xCo_y, Ho_xFe_y) Intermetallic Compounds in Chloride Melts. *Processes* **2022**, *10*, 1723. [CrossRef]
4. Zeng, Y.; Cui, G.; Wu, W.; Xu, C.; Huang, J.; Wang, J.; Yang, Z. Numerical Simulation Study on Flow Heat Transfer and Stress Distribution of Shell-and-Tube Superheater in Molten Salt Solar Thermal Power Station. *Processes* **2022**, *10*, 1003. [CrossRef]
5. Redkin, A.; Korzun, I.; Reznitskikh, O.; Yaroslavtseva, T.; Zaikov, Y.; Kumkov, S. Heat of Fusion of Halide Salts and their Eutectics. *J. Therm. Anal. Calorim.* **2018**, *131*, 2021–2026. [CrossRef]
6. Carotti, F.; Wu, H.; Scarlat, R.O. Characterization of a Thermodynamic Reference Electrode for Molten LiF–BeF_2 (FLiBe). *J. Electrochem. Soc.* **2017**, *164*, H854–H861. [CrossRef]
7. Ignatiev, V.V.; Merzlyakov, V.A.; Subbotin, V.G.; Panov, A.V. Experimental Study of Physical Properties of Molten Salts Containing Fluorides of Sodium, Lithium and Beryllium Difluoride. *At. Energy* **2006**, *101*, 364–372. [CrossRef]
8. Alekseev, P.N.; Gagarinskii, A.Y.; Kalugin, M.A.; Kukharkin, N.E.; Semchenkov, Y.M.; Sidorenko, V.A.; Subbotin, S.A.; Teplov, P.S.; Fomichenko, P.A.; Asmolov, V.G. On a Strategy for the Development of Nuclear Power in Russia. *At. Energy* **2019**, *126*, 207–219. [CrossRef]
9. Zaikov, Y.P.; Shishkin, V.Y.; Potapov, A.M.; Dedyukhin, A.E.; Kovrov, V.A.; Kholkina, A.S.; Volkovich, V.A.; Polovov, I.B. Research and Development of the Pyrochemical Processing for the Mixed Nitride Uranium-Plutonium Fuel. *J. Phys. Conf. Ser.* **2020**, *1475*, 012027. [CrossRef]
10. Kim, S.; Kim, J.; Cho, D.; Bang, S. Quantitative Cost-Benefit Analysis of Direct Disposal and Pyroprocessing in Korea's Nuclear Fuel Cycle. *Sustainability* **2021**, *13*, 7789. [CrossRef]
11. Choi, E.-Y.; Lee, J. Highly Enhanced Reduction of Rare Earth Oxides in Simulated Oxide Fuel in Li_2O–LiCl Salt Using Lithium Metal. *J. Nucl. Mat.* **2018**, *511*, 367–374. [CrossRef]
12. Sakamura, Y.; Murakami, T.; Tada, K.; Kitawaki, S. Electrowinning of U–Pu onto Inert Solid Cathode in LiCl–KCl Eutectic Melts Containing UCl_3 and $PuCl_3$. *J. Nucl. Mat.* **2018**, *502*, 270–275. [CrossRef]
13. Pitchaiah, K.C.; Sujatha, K.; Deepitha, J.; Ghosh, S.; Sivaraman, N. Recovery of Uranium and Plutonium from Pyrochemical Salt Matrix Using Supercritical Fluid Extraction. *J. Supercrit. Fluids* **2019**, *147*, 194–204. [CrossRef]
14. Kim, S.; Ko, W.; Bang, S. Analysis of Unit Process Cost for an Engineering-Scale Pyroprocess Facility Using a Process Costing Method in Korea. *Energies* **2015**, *8*, 8775–8797. [CrossRef]
15. Williamson, M.A.; Willit, J.L. Pyroprocessing Flowsheets for Recycling Used Nuclear Fuel. *Nucl. Eng. Technol.* **2011**, *43*, 329–333. [CrossRef]
16. Karfidov, E.A.; Zaikov, Y.P.; Nikitina, E.V.; Seliverstov, K.E.; Dub, A.V. High-Temperature Passivation of the Surface of Candidate Materials for MSR by Adding Oxygen Ions to FLiNaK Salt. *Materials* **2022**, *15*, 5174. [CrossRef]
17. Arkhipov, S.P.; Zaikov, Y.P.; Arkhipov, P.A.; Mullabaev, A.R. Interaction between Iron Fluoride and Molten FLiBe. *Processes* **2022**, *10*, 2742. [CrossRef]
18. Swain, L.; Ghosh, S.; Pakhui, G.; Prabhakara Reddy, B. Redox Behavior of Moisture in LiCl–KCl Eutectic Melts: A Cyclic Voltammetry Study. *Nucl. Technol.* **2021**, *207*, 119–146. [CrossRef]
19. Tian, W. Grand Challenges in Advanced Nuclear Reactor Design. Front. *Nucl. Eng.* **2022**, *1*, 1000754. [CrossRef]
20. Redkin, A.; Il'ina, E.; Pershina, S.; Mushnikov, P.; Stankus, S.; Agazhanov, A.; Zaikov, Y.; Kholkina, A.; Artamonov, A. Thermal Properties of Li_2BeF_4 near Melting Point. *Thermo* **2022**, *2*, 107–115. [CrossRef]
21. Salyulev, A.B.; Moskalenko, N.I.; Shishkin, V.Y.; Zaikov, Y.P. Selective Evaporation of the Components of Molten $(LiCl–KCl)_{eut}$–$BaCl_2$–$SrCl_2$–$NdCl_3$ Mixtures at Low Pressures. *Rus. Met.* **2021**, *2021*, 151–158. [CrossRef]
22. Laitinen, H.A.; Ferguson, W.S.; Osteryoung, R.A. Preparation of Pure Fused Lithium Chloride-Potassium Eutectic Solvent. *J. Electrochem. Soc.* **1957**, *104*, 516. [CrossRef]
23. Suzdaltsev, A.V.; Filatov, A.A.; Nikolaev, A.Y.; Pankratov, A.A.; Molchanova, N.G.; Zaikov, Y.P. Extraction of Scandium and Zirconium from Their Oxides during the Electrolysis of Oxide−Fluoride Melts. *Rus. Met.* **2018**, *2018*, 133–138. [CrossRef]
24. Chernyshev, A.A.; Arkhipov, S.P.; Apisarov, A.P.; Shmygalev, A.S.; Isakov, A.V.; Zaikov, Y.P. Rhenium Electrodeposition and Its Electrochemical Behavior in Molten KF–KBF_4–B_2O_3–$KReO_4$. *Materials* **2022**, *15*, 8679. [CrossRef]

25. Shishkin, A.V.; Shishkin, V.Y.; Pankratov, A.A.; Burdina, A.A.; Zaikov, Y.P. Electrochemical Reduction of La_2O_3, Nd_2O_3, and CeO_2 in LiCl–Li_2O Melt. *Materials* **2022**, *15*, 3963. [CrossRef]
26. Nikolaev, A.Y.; Mullabaev, A.R.; Suzdaltsev, A.V.; Kovrov, V.A.; Kholkina, A.S.; Shishkin, V.Y.; Zaikov, Y.P. Purification of Alkali-Metal Chlorides by Zone Recrystallization for the Use in Pyrochemical Processing of Spent Nuclear Fuel. *At. Energy* **2022**, *131*, 195–201. [CrossRef]
27. Suzdaltsev, A. Silicon Electrodeposition for Microelectronics and Distributed Energy: A Mini-Review. *Electrochem* **2022**, *3*, 760–768. [CrossRef]
28. Kosov, A.V.; Semerikova, O.L.; Vakarin, S.V.; Grishenkova, O.V.; Vorob'ev, A.S.; Khudorozhkova, A.O.; Zaikov, Y.P. Ionic Equilibria in Polytungstate Melts. *Processes* **2022**, *10*, 2658. [CrossRef]
29. Rudenko, A.; Redkin, A.; Il'ina, E.; Pershina, S.; Mushnikov, P.; Zaikov, Y.; Kumkov, S.; Liu, Y.; Shi, W. Thermal Conductivity of FLiNaK in a Molten State. *Materials* **2022**, *15*, 5603. [CrossRef]
30. Gevel, T.; Zhuk, S.; Leonova, N.; Leonova, A.; Trofimov, A.; Suzdaltsev, A.; Zaikov, Y. Electrochemical Synthesis of Nano-Sized Silicon from KCl–K_2SiF_6 Melts for Powerful Lithium-Ion Batteries. *Appl. Sci.* **2021**, *11*, 10927. [CrossRef]
31. Zheng, J.; Sahoo, S.K.; Aono, T. Recent Progress on Mass Spectrometric Analysis of Artificial Radionuclides in Environmental Samples Collected in Japan. *Nucl. Anal.* **2022**, *1*, 100025. [CrossRef]
32. Suárez-Oubiña, C.; Herbello-Hermelo, P.; Bermejo-Barrera, P.; Moreda-Piñeiro, A. Exploiting Dynamic Reaction Cell Technology for Removal of Spectral Interferences in the Assessment of Ag, Cu, Ti, and Zn by Inductively Coupled Plasma Mass Spectrometry. *Spectrochim. Acta Part B At. Spectrosc.* **2022**, *187*, 106330. [CrossRef]
33. Panchuk, V.; Petrov, Y.; Semenov, V.; Kirsanov, D. Quantification of Elements in Spent Nuclear Fuel Using Intrinsic Radioactivity for Sample Excitation and Chemometric Data Processing. *Anal. Chim. Acta* **2023**, *1239*, 340694. [CrossRef]
34. Santos, J.S.; Teixeira, L.S.G.; Santos, W.N.L.; Lemos, V.A.; Sérgio, J.M.G.; Ferreira, L.C. Uranium Determination Using Atomic Spectrometric Techniques: An Overview. *Anal. Chim. Acta* **2010**, *674*, 143–156. [CrossRef]
35. Mullabaev, A.R.; Kovrov, V.A.; Kholkina, A.S.; Zaikov, Y.P. Anode Processes on Pt and Ceramic Anodes in Chloride and Oxide-Chloride Melts. *Nucl. Eng. Techn.* **2022**, *54*, 965–974. [CrossRef]
36. Guo, X.; Sun, Z.; Sietsma, J.; Blanpain, B.; Guo, M.; Yang, Y. Quantitative Study on Dissolution Behavior of Nd_2O_3 in Fluoride Melts. *Ind. Eng. Chem. Res.* **2018**, *57*, 1380–1388. [CrossRef]
37. Nikolaev, A.Y.; Pavlenko, O.B.; Suzdaltsev, A.V.; Zaikov, Y.P. Electrochemical Sensor for Monitoring the Alumina Dissolution and Concentration in a Cryolite-Alumina Melt. *J. Electrochem. Soc.* **2020**, *167*, 126511. [CrossRef]
38. Senanu, S.; Ratvik, A.P.; Gudbrandsen, H.; Martinez, A.M.; Store, A.; Gebarowski, W. Dissolution and Online Monitoring of Nd and Pr Oxides in NdF_3–PrF_3–LiF Electrolytes. *Metals* **2021**, *11*, 326. [CrossRef]
39. Peng, H.; Huang, W.; Xie, L.; Li, Q. Solubility and Precipitation Investigations of UO_2 in LiF–BeF_2 Molten Salt. *J. Nucl. Mat.* **2020**, *531*, 152004. [CrossRef]
40. Choi, E.-Y.; Choi, I.-K.; Hur, J.-M.; Kang, D.-S.; Shin, H.-S.; Jeong, S.M. In Situ Electrochemical Measurement of O^{2-} Concentration in Molten Li_2O/LiCl During Uranium Oxide Reduction Process. *Electrochem. Solid-State Lett.* **2012**, *15*, E11–E13. [CrossRef]
41. Zhang, H.; Choi, S.; Zhang, C.; Faulkner, E.; Alnajjar, N.; Okabe, P.; Horvath, D.C.; Simpson, M.F. Square Wave Voltammetry for Real Time Analysis of Minor Metal Ion Concentrations in Molten Salt Reactor Fuel. *J. Nucl. Mat.* **2019**, *527*, 151791. [CrossRef]
42. Pershin, P.S.; Suzdaltsev, A.V.; Zaikov, Y.P. Dissolution of Al_2O_3 in KF–AlF_3. *Rus. Met.* **2021**, *2021*, 213–218. [CrossRef]
43. Cvetkovic, V.S.; Feldhaus, D.; Vukicevic, N.M.; Milicevic-Neumann, K.; Barudžija, T.S.; Friedrich, B.; Jovicevic, J.N. Influence of Rare Earth Oxide Concentration on Electrochemical Co-Deposition of Nd and Pr from NdF_3–PrF_3–LiF Based Melts. *Metals* **2022**, *12*, 1204. [CrossRef]
44. Valtseva, A.I.; Pershin, P.S.; Kalyakin, A.S.; Volkov, A.N.; Suzdaltsev, A.V.; Zaikov, Y.P. Development of Oxygen Sensor for Pyrochemical Reactors of Spent Nuclear Fuel Reprocessing. *J. Phys. Conf. Ser.* **2020**, *1565*, 012050. [CrossRef]
45. Suzdaltsev, A.V.; Nikolaev, A.Y.; Pavlenko, O.B.; Zaikov, Y.P. Monitoring Alumina Content in Cryolite-Alumina melt. *IOP Conf. Ser. Mat. Sci. Eng.* **2020**, *918*, 012108. [CrossRef]
46. Shen, M.; Peng, H.; Ge, M.; Zuo, Y.; Xie, L. Use of Square Wave Voltammeter for Online Monitoring of O2- Concentration in Molten Fluorides at 600 °C. *J. Electroanal. Chem.* **2015**, *748*, 34–39. [CrossRef]
47. Nibedita, S.; Satendra, K.; Maji, S.; Chandra, M.; Venkatesh, P.; Jain, A. Electrochemical and Spectroscopic Analysis of Thermochemical Conversion of UO_2 to UCl_3 Using $AlCl_3$ and Al in LiCl–KCl Eutectic. *Progr. Nucl. Energy* **2022**, *153*, 104429. [CrossRef]
48. Song, Y.; Shen, M.; Zhao, S.; Tang, R.; Xie, L.; Qian, Y. Interactions Between Oxide and LiF–BeF_2–ZrF_4–UF_4 System through Electrochemical Techniques. *J. Electrochem. Soc.* **2021**, *168*, 036513. [CrossRef]
49. Pershin, P.; Khalimullina, Y.; Arkhipov, P.; Zaikov, Y. The Electrodeposition of Lead in LiCl–KCl–$PbCl_2$ and LiCl–KCl–$PbCl_2$–PbO Melts. *J. Electrochem. Soc.* **2014**, *161*, D824–D830. [CrossRef]
50. Haarberg, G.M.; Owe, L.-E.; Qin, B.; Wang, J.; Tunold, R. Electrodeposition of Lead from Chloride Melts. *ECS Trans.* **2012**, *50*, 215–219. [CrossRef]
51. Arkhipov, P.A.; Zaikov, Y.P.; Khalimullina, Y.R.; Arkhipov, S.P. Electrochemical Production of Bismuth in the KCl–$PbCl_2$ Melt. *Materials* **2021**, *14*, 5653. [CrossRef]
52. Zhu, Z.-L.; Liu, H.; Chen, J.-S.; Kong, H.; Xu, L.; Hua, Z.-S.; Zhao, Z. Electrochemical Behavior and Electrolytic Preparation of Lead in Eutectic NaCl−KCl Melts. *Trans. Nonferrous Met. Soc. China* **2020**, *30*, 2568–2576. [CrossRef]

53. Pershin, P.S.; Kataev, A.A.; Shurov, N.I.; Arkhipov, P.A.; Zaikov, Y.P. Dissolution Rate of Lead(II) Oxide in an Equimolar KCl-$PbCl_2$ Melt. *Rus. J. Non-Ferr. Met.* **2013**, *54*, 195–200. [CrossRef]
54. Zhitkov, A.; Potapov, A.; Karimov, K.; Shishkin, V.; Dedyukhin, A.; Zaykov, Y. Interaction Between UN and $CdCl_2$ in Molten LiCl–KCl Eutectic. I. Experiment at 773 K. *Nucl. Eng. Techn.* **2020**, *52*, 123–134. [CrossRef]
55. Nikolaev, A.Y.; Suzdaltsev, A.V.; Zaikov, Y.P. High Temperature Corrosion of ZrN Powder in Molten LiCl with Additions of $PbCl_2$, KCl, Li_2O, H_2O, and LiOH. *J. Electrochem. Soc.* **2019**, *166*, C147–C152. [CrossRef]
56. Shchepin, A.S.; Koshcheev, A.M.; Kalenova, M.Y.; Melnikova, I.M. SNF Processing Electrochemical Operations: Liquid-Metal and Salt Medium Purification. *Izv. Vuzov. Yad. Energ.* **2021**, *4*, 53–65. (In Russian) [CrossRef]
57. Kizub, P.A.; Blokhin, A.I.; Blokhin, P.A.; Mitenkova, E.F.; Mosunova, N.A.; Kovrov, V.A.; Shishkin, A.V.; Zaikov, Y.P.; Rakhmanova, O.R. Criticality Analysis of Pyrochemical Reprocessing Apparatuses for Mixed Uranium-Plutonium Nitride Spent Nuclear Fuel Using the MCU-FR and MCNP Program Codes. *Nucl. Eng. Techn.* **2023**. [CrossRef]
58. Swain, N.; Soni, I.; Kumar, P.; Kudur Jayaprakash, G. Electrochemical Reduction and Voltammetric Sensing of Lindane at the Carbon (Glassy and Pencil) Electrodes. *Electrochemistry* **2022**, *3*, 248–258. [CrossRef]
59. Nikolaev, A.Y.; Pavlenko, O.B.; Suzdaltsev, A.V.; Zaikov, Y.P.; Vykhoteds, V.B.; Kurennykh, T.E. Reduction of ZrO_2 During the SNF Pyroprocessing. *J. Electrochem. Soc.* **2021**, *168*, 036506. [CrossRef]
60. Volkov, V.N.; Vykhodets, V.B.; Golubkov, I.K.; Klotsman, S.M.; Lerkh, P.V.; Pavlov, V.A. Accurate Light Ion Beam Monitoring by Backscattering. *Nucl. Instrum. Methods Phys. Res.* **1983**, *205*, 73. [CrossRef]
61. Vykhodets, V.B.; Kurennykh, T.E.; Vykhodets, E.V. Disks of Oxygen Vacancies on the Surface of TiO_2 Nanoparticles. *Appl. Sci.* **2022**, *12*, 11963. [CrossRef]
62. Suzdaltsev, A.V.; Nikolaev, A.Y.; Zaikov, Y.P. Towards the Stability of Low-Temperature Aluminum Electrolysis. *J. Electrochem. Soc.* **2021**, *168*, 046521. [CrossRef]
63. Mohamedi, M.; Børresen, B.; Haarberg, G.M.; Tunold, R. Anodic Behavior of Carbon Electrodes in CaO–$CaCl_2$ Melts at 1123 K. *J. Electrochem. Soc.* **1999**, *146*, 1472–1477. [CrossRef]
64. Roine, A. *HSC Chemistry® 9.0*; Outotec: Pori, Finland, 2018. Available online: www.outotec.com/HSC (accessed on 1 January 2021).
65. Zakiryanova, I.D.; Arkhipov, P.A.; Zakiryanov, D.O. Reaction Mechanism of Lead (II) Oxide with a $PbCl_2$–CsCl Melt According to Raman Spectroscopic Data. *J. Appl. Spectrosc.* **2016**, *82*, 920–924. [CrossRef]